

Phenomenological model for long-wavelength optical modes in transition metal dichalcogenide monolayer

C. Trallero-Giner ¹, E. Menéndez-Proupin ^{2,3}, E. Suárez Morell ⁴, R. Pérez-Álvarez ⁵, and Darío G. Santiago-Pérez ⁶

¹*Department of Theoretical Physics, Havana University, Havana 10400, Cuba*

²*Departamento de Física Aplicada I, Escuela Politécnica Superior, Universidad de Sevilla, Sevilla E-41011, Spain*

³*Departamento de Física, Facultad de Ciencias, Universidad de Chile, Santiago 780-0003, Chile*

⁴*Departamento de Física, Universidad Técnica, Federico Santa María, Casilla 110-V, Valparaíso 2340000, Chile*

⁵*Universidad Autónoma del Estado de Morelos, Ave. Universidad 1001, Cuernavaca, Morelos CP 62209, México*

⁶*Departamento de Física Matemática, Universidad de Sancti Spiritus “José Martí Pérez”, Ave. de los Mártires 360, Sancti Spiritus CP 62100, Cuba*



(Received 24 April 2021; accepted 7 June 2021; published 21 June 2021)

Transition metal dichalcogenides (TMDs) are an exciting family of 2D materials; a member of this family, MoS₂, became the first studied monolayer semiconductor. In this paper, a generalized phenomenological continuum approach for the optical vibrations of the monolayer TMDs valid in the long-wavelength limit is developed. The equation of motions for nonpolar and polar oscillations include the phonon dispersion up to a quadratic approximation in the phonon wave vector. On the other hand, the polar modes satisfy coupled equations for the displacement vector and the inner electric field. The two-dimensional phonon dispersion curves for in-plane and out-of-plane oscillations are thoroughly analyzed. The model parameters are fitted from density functional perturbation theory calculations. The current formalism provides an effective tool to describe the phonon dispersion curves around the Γ point of the Brillouin zone for a large group of members of the TMD monolayers. A detailed evaluation of the intravalley Pekar-Fröhlich and the A_1 -homopolar mode deformation potential coupling mechanisms is performed. The effects of metal ions and chalcogen atoms on polaron mass and binding energy are studied. It is argued that both mechanisms should be considered for a correct analysis of the properties of the polaron or of any process that involves the intraband transitions assisted by the electron-phonon interaction.

DOI: [10.1103/PhysRevB.103.235424](https://doi.org/10.1103/PhysRevB.103.235424)

I. INTRODUCTION

The emergence of two-dimensional (2D) transition metal dichalcogenide (TMD) materials has encouraged basic research with potentially extraordinary applications in the field of energy storage, biosensors, electronic devices, solar cells, among others (see Refs. [1–4]). The bulk family of TMDs has a puckered layered structure with a MX₂ pattern in each layer, M=Mo, W is a transition metal, and X=S, Se, Te a chalcogen. The stacking can be found preferably forming three different polytypes with 2H hexagonal honeycomb, 1T trigonal, or 3R rhombohedral symmetries. These structures include semimetals such as MoTe₂ and WTe₂ or semiconductors like MoS₂, MoSe₂, WS₂, and WSe₂ [5]. Molybdenum disulfide monolayer (1ML) is the most studied member of this family [6]. Due to the existence in the 1ML MoS₂ of a direct band gap of 1.75 eV, the TMD family acquired a renewed notoriety with promising applications in optoelectronics. It has been shown that optical phonons of the 1ML TMD impact the interband and intraband relaxation processes [7], transport properties [8,9], photoluminescence [10], hot luminescence [11], and even modulate the piezoelectricity effect [12]. In addition, the phonon-assisted exciton recombination explains the observed photoluminescence peaks below the bright exciton of WSe₂. The developed microscopic model includes both the inter- and

intravalley exciton scattering assisted by optical and acoustic phonons [13].

In general, in any comprehensive study of dielectric and electronic properties of 2D TMDs the role of the optical phonons needs to be addressed [14]. In the phonon spectra of 1ML TMDs we can find six optical branches at the Γ point of the Brillouin zone (BZ) that are classified in terms of the irreducible representation of the point group D_{3h} [15–17] with symmetries E'' (LO₁ and TO₁), E' (LO₂ and TO₂), A_1 (ZO₂), and A_2 (ZO₁) which correspond to two in-plane longitudinal (LO₁ and LO₂), two in-plane transverse (TO₁ and TO₂), and two out-of-plane (ZO₁ and ZO₂) vibrations.

The development of analytical methods together with *ab initio* calculations allows us to describe optical oscillations in 2D materials and understand phonon dispersion laws [18] as well as the electron-phonon interaction [19]. A phenomenological continuum model should contain the symmetry properties of the structure and the main characteristics of the optical modes under study. In this paper, we present a long-wavelength phenomenological continuum approach for the six optical phonon branches of the 2D TMD family. The formalism takes into account the dispersion up to quadratic dependence on the phonon wave vector and the symmetry properties. We assume in-plane isotropy, as the anisotropy

derived from the D_{3h} symmetry is negligible in the dispersion laws for long wavelength. This results in six analytical solutions for the optical branches. The parameters introduced in the equation of motions were fitted to match *ab initio* calculations of the phonon spectra. The polaronic corrections are also obtained considering both Fröhlich and short-range deformation potential interactions, emphasizing the important role of the A_1 -homopolar mode. Our model provides an easy approach to get an accurate description of the in-plane and out-of-plane phonon properties of all the TMD family.

The paper is organized as follows: In Sec. II we introduce the phenomenological model starting from a general equation of motion for the relative displacement vector of the atoms involved in the phonon oscillations. In Sec. III we describe the procedure we followed with the *ab initio* calculations of the TMDs. In Sec. IV we list all the parameters of our phenomenological macroscopic approach for all the family of TMD obtained from fitting *ab initio* calculations and elaborate on LO₂-TO₂ splitting found in the optical modes. In Sec. V we derive analytically two main mechanisms responsible for the electron-phonon interaction: Pekar-Fröhlich and A_1 -homopolar deformation potential interactions. In Sec. VI employing both Hamiltonians, we explore the polaron properties and obtain the polaron mass and binding energy. Finally, we expose our conclusions in Sec. VII.

II. PHENOMENOLOGICAL MODEL

Lets recall first some basic concepts of the long-wavelength phenomenological continuum approach adapted to 2D TMD layers [21]. For the sake of clarity, we divide the study of the six optical oscillations into two groups: (i) polar modes with E' (LO₂, TO₂) or A_2 (ZO₁) symmetry and (ii) nonpolar phonons for the E'' (LO₁, TO₁) or A_1 (ZO₂) branches.

A. Polar phonons

The opposite motions of chalcogen (X_i , $i = 1, 2$) and transition-metal (M) ions are responsible for the appearance of three polar branches. The oscillations are composed of the in-plane (LO₂, TO₂) and out-of-plane (ZO₂) modes with a relative vector displacement $\mathbf{U} = \mathbf{u}_M - (\mathbf{u}_{X_1} + \mathbf{u}_{X_2})/2$ where \mathbf{u}_M (\mathbf{u}_{X_i} , $i = 1, 2$) is the vector amplitude of the metal (chalcogen). Hence, the normal vibrational mode at Γ with irreducible representation A_2 is infrared active while E' is Raman and infrared active [16]. These atomic displacements in the unit cell generate a macroscopic electric field \mathbf{E} in the layer. We will assume the following equation of motion for the relative vector displacement $\mathbf{U} = (\mathbf{u}_{E'}(\boldsymbol{\rho}), u_{z_{O_1}}(\boldsymbol{\rho}))$ of the atoms involved in the long-wavelength limit for polar phonons around the Γ point of the BZ,

$$\rho_m \omega^2 \mathbf{U} + \vec{\gamma} \cdot \mathbf{U} + \vec{\alpha} \cdot \mathbf{E}(\boldsymbol{\rho}, 0) - \nabla \cdot \vec{\sigma} = 0, \quad (1)$$

where ρ_m is the 2D reduced mass density with $\mu^{-1} = m_M^{-1} + (2m_X)^{-1}$, $\mathbf{E}(\boldsymbol{\rho}, 0) = (\mathbf{E}_\rho(\boldsymbol{\rho}, 0), E_z(\boldsymbol{\rho}, 0))$ the 2D electric field and $\boldsymbol{\rho}$ the in-plane radius vector. In Eq. (1) $\vec{\gamma}$, $\vec{\alpha}$, $\vec{\sigma}$ are second rank tensors. $\vec{\gamma}$ is a symmetric tensor describing the coupling

of mechanical amplitude with itself given by

$$\vec{\gamma} = -\rho_m \begin{pmatrix} \omega_{E'}^2 & 0 & 0 \\ 0 & \omega_{E'}^2 & 0 \\ 0 & 0 & \omega_{0A_2}^2 \end{pmatrix}, \quad (2)$$

$\omega_{E'}$ (ω_{0A_2}) being the natural optical frequency at in-plane (out-of-plane) phonon wave vector $\mathbf{q} = \mathbf{0}$ with symmetry E' (A_2). The tensor $\vec{\alpha}$ describes the interaction between the mechanical vector amplitude \mathbf{U} and the field \mathbf{E} expressed in the form

$$\vec{\alpha} = \begin{pmatrix} \alpha & 0 & 0 \\ 0 & \alpha & 0 \\ 0 & 0 & \alpha_{z_{O_1}} \end{pmatrix}, \quad (3)$$

where α ($\alpha_{z_{O_1}}$) is the coupling constant between the displacement $\mathbf{u}_{E'}(\boldsymbol{\rho})$ [$u_{z_{O_1}}(\boldsymbol{\rho})$] and the in-plane macroscopic electric field $\mathbf{E}_\rho(\boldsymbol{\rho}, 0)$ [the z component of the electric field, $E_z(\boldsymbol{\rho}, 0)$]. The term $\nabla \cdot \vec{\sigma}$ is introduced to describe the phonon dispersion up to the quadratic term in the phonon wave vector and it can be cast as (see Appendix A)

$$\nabla \cdot \vec{\sigma} = \rho_m \begin{pmatrix} \mp \beta_{LO_2}^2 \partial_x^2 u_x \mp \beta_{TO_2}^2 \partial_y^2 u_x \pm (\beta_{LO_2}^2 - \beta_{TO_2}^2) \partial_{x,y}^2 u_y \\ \mp \beta_{LO_2}^2 \partial_y^2 u_y \mp \beta_{TO_2}^2 \partial_x^2 u_y \pm (\beta_{LO_2}^2 - \beta_{TO_2}^2) \partial_{x,y}^2 u_x \\ \mp \beta_{z_{O_1}}^2 (\partial_x^2 u_z + \partial_y^2 u_z) \end{pmatrix}. \quad (4)$$

The coefficients α , $\alpha_{z_{O_1}}$, β_{LO_2} , β_{TO_2} , and $\beta_{z_{O_1}}$ are phenomenological parameters obtained by fitting the phonon dispersion law $\omega(\mathbf{q})$ (experimentally or by *ab initio* calculations). The choice of sign, + or -, depends on the curvature of the mode under consideration. In addition, Eq. (1) is supplemented by the Maxwell equation

$$\nabla \cdot (\mathbf{E}(\boldsymbol{\rho}, z) + 4\pi \mathbf{P}(\boldsymbol{\rho}, z)) = 0 \quad (5)$$

for the in-plane oscillations and

$$\nabla \cdot (\mathbf{E}_z(\boldsymbol{\rho}, z) + 4\pi \mathbf{P}_z(\boldsymbol{\rho}, z)) = 0 \quad (6)$$

for the out-of-plane vibrations. For the macroscopic polarizations we assume the following relations

$$\mathbf{P} = [\alpha \mathbf{u}_{E'}(\boldsymbol{\rho}) + \alpha_2 \mathbf{E}_\rho(\boldsymbol{\rho}, 0)] p(z) \quad (7)$$

and

$$\mathbf{P}_z = [\alpha_{z_{O_1}} \mathbf{u}_{z_{O_1}}(\boldsymbol{\rho}) + \chi_e \mathbf{E}_z(\boldsymbol{\rho}, 0)] p(z), \quad (8)$$

where α_2 is the polarizability in the plane and χ_e the out-of-plane electronic susceptibility [18]. The function $p(z)$ in Eqs. (7) and (8) is the profile density along the z direction [8,19,20] and it will be considered uniform over the monolayer of thickness d , i.e.,

$$p(z) = \begin{cases} 1/d & ; \quad |z| < d/2 \\ 0 & ; \quad |z| > d/2. \end{cases} \quad (9)$$

The dispersion relations are obtained by solving the coupled equations (1), (5), and (6) for $\mathbf{u}_{E'}$, $u_{z_{O_1}}$, $\mathbf{E}_\rho(\boldsymbol{\rho}, 0)$, and $\mathbf{E}_z(\boldsymbol{\rho}, 0)$. These equations represent a generalization of the Born-Huang equation [21,22] for 2D TMD materials including the quadratic dependence on the \mathbf{q} vector of the optical modes. Due to the translational symmetry on the plane we have that $\mathbf{U} = (\mathbf{u}_{0E'}, u_{z_{O_1}}) e^{i\mathbf{Q}\cdot\boldsymbol{\rho}}$ and $\mathbf{E}(\boldsymbol{\rho}, z = 0) = \mathbf{E}(\mathbf{q}) e^{i\mathbf{Q}\cdot\boldsymbol{\rho}}$, thus Eq. (1) is decoupled into two independent

equations for in-plane and out-of-plane motions with the vector displacements $\mathbf{u}_1 = (\mathbf{u}_{E'}(\boldsymbol{\rho}), 0)$ and $\mathbf{u}_2 = (0, u_{z_{O_1}}(\boldsymbol{\rho}))$, respectively. As a consequence, we get three phonon dispersion relations, two for in-plane longitudinal (LO₂) and transverse (TO₂) branches with symmetry E' , as well as one for out-of-plane phonon vibration A_2 (ZO₁). Hence, from Eqs. (1) and (5) and using $\mathbf{E}(\boldsymbol{\rho}, z) = -\nabla\varphi(\boldsymbol{\rho}, z)$ we get for the in-plane oscillations

$$\rho_m(\omega^2 - \omega_{E'}^2)\mathbf{u}_{0E'} = -\alpha\mathbf{E}\boldsymbol{\rho}(\mathbf{q}) \pm \rho_m\beta_{LO_2}^2\mathbf{q}(\mathbf{q} \cdot \mathbf{u}_{0E'}) \pm \rho_m\beta_{TO_2}^2[-\mathbf{q}(\mathbf{q} \cdot \mathbf{u}_{0E'}) + q^2\mathbf{u}_{0E'}], \quad (10)$$

and the Poisson' equation

$$\nabla^2\varphi + 4\pi\alpha_2\nabla^2\varphi_2(\boldsymbol{\rho})p(z) = 4\pi\alpha\nabla \cdot [\mathbf{u}_{E'}(\boldsymbol{\rho})p(z)], \quad (11)$$

with $\varphi_2(\mathbf{q}) = \varphi(\boldsymbol{\rho}, z = 0)$. For searching the solution of the system of Eqs. (10) and (11) we take the Fourier transform [23]

$$\varphi(\boldsymbol{\rho}, z) = \frac{1}{(2\pi)^3} \int \bar{\varphi}(\mathbf{q}, q_z) e^{i(\mathbf{q}\cdot\boldsymbol{\rho} + q_z z)} d^2q dq_z. \quad (12)$$

Inserting (12) into (11) we have, in the long-wavelength limit $qd/2 \ll 1$, that the Fourier transform of the electrostatic potential is [24]

$$\bar{\varphi}(\mathbf{q}) = -\frac{2\pi}{q} \frac{\alpha F(\mathbf{q})}{1 + 2\pi\alpha_2 q}, \quad (13)$$

where $\bar{\varphi}(\mathbf{q}) = \int_{-\infty}^{\infty} \bar{\varphi}(\mathbf{q}, q_z) dq_z/2\pi$ and

$$F(\mathbf{q}) = \int \nabla \cdot [\mathbf{u}_{E'}(\boldsymbol{\rho}) e^{-i\mathbf{q}\cdot\boldsymbol{\rho}}] d^2\rho. \quad (14)$$

From the Fourier transform of the in-plane electric field $\mathbf{E}\boldsymbol{\rho}(\boldsymbol{\rho}, z = 0) = -\nabla\varphi_2(\boldsymbol{\rho})$ we get from (13) and (14)

$$\mathbf{E}(\mathbf{q}) = -2\pi\alpha \frac{\mathbf{q} \cdot \mathbf{u}_{0E'}}{q(1 + 2\pi\alpha_2 q)}. \quad (15)$$

Employing (10) and (15) and considering $\mathbf{u}_{0E'} = \mathbf{u}_{LO_2} + \mathbf{u}_{TO_2}$, with \mathbf{u}_{LO_2} (\mathbf{u}_{TO_2}) the longitudinal (transverse) vector displacement, we obtain that the phonon dispersion relation for the LO₂ phonon is given by

$$\omega^2 = \omega_{E'}^2 + \frac{2\pi\alpha^2}{\rho_m} \frac{q}{(1 + 2\pi\alpha_2 q)} \pm \beta_{LO_2}^2 q^2, \quad (16)$$

and for TO₂ mode

$$\omega^2 = \omega_{E'}^2 \pm \beta_{TO_2}^2 q^2. \quad (17)$$

We observe that the breaking of the translational symmetry along the z axis provokes the absence of LO₂-TO₂ splitting at Γ ; the LO₂ and TO₂ phonons are degenerate at $\mathbf{q} = \mathbf{0}$. The LO₂ mode is due to the longitudinal displacement and its dispersion relation (16) shows a finite slope. The coupling of the LO₂ phonon amplitude with the macroscopic electric field (15) is responsible of the q -linear behavior at the long-wavelength limit.

In the out-of-plane A_2 vibration, Eqs. (1) and (6) provide the macroscopic equations

$$\rho_m(\omega^2 - \omega_{A_2}^2)u_{z_{O_1}} = -\alpha_{z_{O_1}}E_z(\mathbf{q}) \mp \rho_m\beta_{z_{O_1}}^2 q^2 u_{z_{O_1}} \quad (18)$$

and

$$\left[\frac{d^2}{dz^2} - q^2 \right] \varphi_0(z) = 4\pi \frac{dp}{dz} \left[\alpha_{z_{O_1}} u_{0z} - \chi_e \frac{d\varphi_0(0)}{dz} \right], \quad (19)$$

where the electrostatic potential is chosen as $\varphi(\boldsymbol{\rho}, z) = \varphi_0(z) e^{i\mathbf{q}\cdot\boldsymbol{\rho}}$. Taking $\varphi_0(z) = \int_{-\infty}^{\infty} \bar{\varphi}(q_z) e^{iq_z z} dz/2\pi$ and employing Eq. (19) follows in the $qd/2 \ll 1$ limit that the z component of the electric field $E_z(\mathbf{q})$ is written as [23]

$$E_z = -\frac{4\pi}{d} \frac{\alpha_{z_{O_1}}}{1 + \frac{4\pi}{d}\chi_e} u_{z_{O_1}}. \quad (20)$$

Employing Eqs. (20) and (18) we have the phonon dispersion for the A_2 mode

$$\omega^2 = \omega_{A_2}^2 + \frac{4\pi}{\rho_m d} \frac{\alpha_{z_{O_1}}^2}{(1 + \frac{4\pi}{d}\chi_e)} \mp \beta_{z_{O_1}}^2 q^2. \quad (21)$$

The role of the coupling constant term $\alpha_{z_{O_1}}$ and the electronic susceptibility χ_e is to renormalize the intrinsic oscillatory frequency ω_{0A_2} , thus

$$\omega^2 = \omega_{A_2}^2 \mp \beta_{z_{O_1}}^2 q^2. \quad (22)$$

We take $\omega_{A_2}^2 = \omega_{0A_2}^2 + 4\pi\alpha_{z_{O_1}}^2 / [\rho_m d (1 + \frac{4\pi}{d}\chi_e)]$ equal to the frequency value at $q = 0$ provided by *ab initio* calculations.

B. Nonpolar phonons

The modes with symmetry E'' are responsible for one-in-plane longitudinal (LO₁) and one-in-plane transverse (TO₁) optical vibrations, while the A_1 (ZO₂) mode oscillates out of plane. The normal vector displacement $\mathbf{U}_N = (\mathbf{U}_{X_1} - \mathbf{U}_{X_2})/2 = (\mathbf{U}_{E''}, u_{z_{O_2}})$ describes the contrary motion of the two chalcogen atoms X_i ($i = 1, 2$) with the mass of the metal fixed and reduced mass $\mu^{-1} = 2m_X^{-1}$. As a consequence we are in the presence of nonpolar modes independent of the electric field. Both branches are Raman active [18] and fulfill the following equation of motion

$$\rho_m\omega^2\mathbf{U}_N + \vec{\gamma}_N \cdot \mathbf{U}_N - \nabla \cdot \vec{\sigma}_N = \mathbf{0}, \quad (23)$$

where the tensors $\vec{\gamma}_N$ and $\vec{\sigma}_N$ have the same structures as $\vec{\gamma}$ and $\vec{\sigma}$ in Eqs. (2) and (4) but with the substitutions of $\omega_{E'} \rightarrow \omega_{E''}$, $\omega_{0A_2} \rightarrow \omega_{0A_1}$, $\beta_{LO_2} \rightarrow \beta_{LO_1}$, $\beta_{TO_2} \rightarrow \beta_{TO_1}$, and $\beta_{z_{O_1}} \rightarrow \beta_{z_{O_2}}$. As in the polar case, these parameters are evaluated by fitting the dispersion relations obtained from Eq. (23) with experimental values or by *ab initio* calculations. Searching the solutions of Eq. (23) as $\mathbf{U}_N = (\mathbf{u}_{0E''}, u_{z_{O_2}}) e^{i\mathbf{q}\cdot\boldsymbol{\rho}}$ we get for the vector component $\mathbf{u}_{0E''}$ the equation

$$(\omega^2 - \omega_{E''}^2)\mathbf{u}_{0E''} = \pm \beta_{LO_1}^2 \mathbf{q}(\mathbf{q} \cdot \mathbf{u}_{0E''}) \pm \rho_m\beta_{TO_1}^2 [-\mathbf{q}(\mathbf{q} \cdot \mathbf{u}_{0E''}) + q^2\mathbf{u}_{0E''}]. \quad (24)$$

Taking $\mathbf{u}_{0E''} = \mathbf{u}_{LO_1} + \mathbf{u}_{TO_1}$, where \mathbf{u}_{LO_1} and \mathbf{u}_{TO_1} are two independent vector amplitudes, immediately follows the dispersion relations for the longitudinal LO₁ mode

$$\omega^2 = \omega_{E''}^2 \pm \beta_{LO_1}^2 q^2 \quad (25)$$

and

$$\omega^2 = \omega_{E''}^2 \pm \beta_{TO_1}^2 q^2 \quad (26)$$

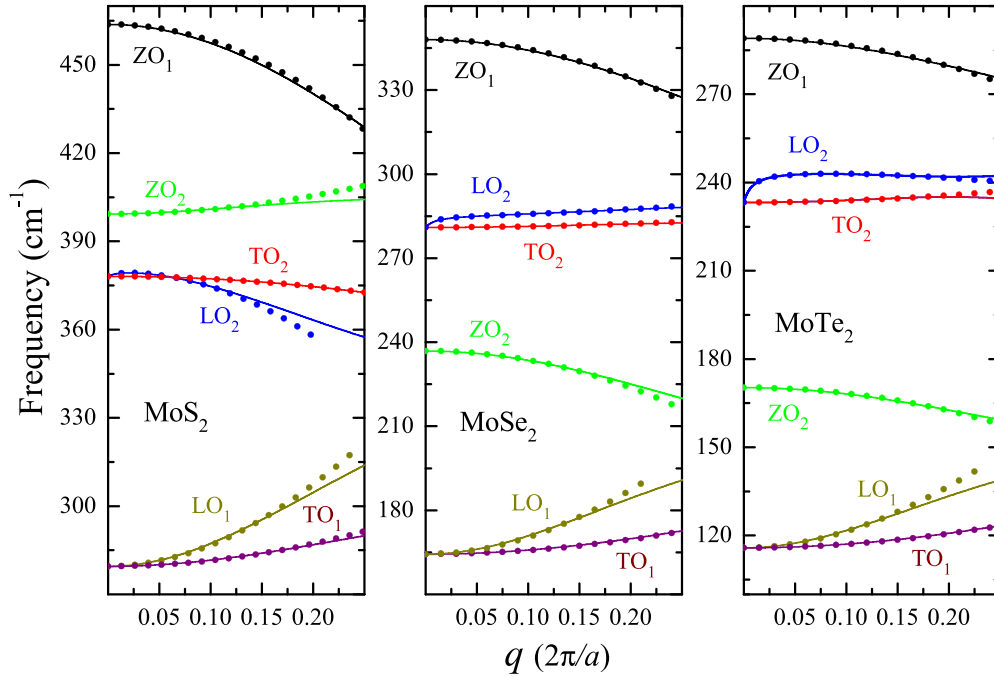


FIG. 1. Optical phonon dispersions for 1ML MoX₂ (X=S, Se, Te). Out-of-plane phonons: A₂(ZO₁) (black) and A₁(ZO₂) (green). In-plane modes with symmetry E'' and E' split into LO₁ (dark yellow), TO₁ (purple), and LO₂ (blue) and TO₂ (red) optical phonons. Straight lines correspond to *ab initio* calculations as explained in Sec. III; dots represent the dispersion laws obtained by the phenomenological model detailed in Sec. II.

for the transverse TO₁ mode. For the case of homopolar phonons vibrating out of plane we have

$$(\omega^2 - \omega_{0A_1}^2)u_{z_{O_2}} = \pm\beta_{z_{O_2}}^2 q^2 u_{z_{O_2}}, \quad (27)$$

with the phonon law

$$\omega^2 = \omega_{0A_1}^2 \mp \beta_{z_{O_2}}^2 q^2. \quad (28)$$

III. FIRST-PRINCIPLES CALCULATIONS

We performed *ab initio* calculations employing density functional theory perturbation (DFPT) [25] within the QUANTUM ESPRESSO code [26] to obtain the phonon dispersion spectra for each of the six monolayer TMDs. DFPT relies upon density functional theory (DFT) evaluation of the electronic ground state. We have employed the optB86b-vdW exchange correlation functional [27,28] to properly consider the van der Waals interaction. The spin-orbit coupling is not included in the calculation. We have sampled the Brillouin zone by means of a Γ -centered $12 \times 12 \times 1$ k -point grid. For the expansion of wave functions and electronic density in plane waves, we have set kinetic energy cutoffs of 65 Ry and 650 Ry, respectively. Only the valence electrons enter explicitly in the calculations. The effect of inner electrons is simulated by means of projector augmented wave (PAW) potentials [29] from the PSLibrary [30]. We have optimized the structures by means of variable-cell relaxation, until the forces and in-plane stress tensor components were smaller than 10^{-3} a.u. and 0.01 kbar, respectively. We set the out-of-plane unit cell size equal to five times the in-plane lattice parameter, in order to simulate the TMD layer as embedded in vacuum. The Coulomb interaction was truncated in the out-of-

plane direction [19], allowing total energy, forces, and stresses to be computed in a two-dimensional framework. In our DFPT calculations, we computed the dynamical matrices for a Γ -centered $6 \times 6 \times 1$ q -point grid in the reciprocal lattice unit cell, and we employed Fourier interpolation for intermediate q points. Finally, we obtained phonon frequencies and eigenvectors by diagonalization of the dynamical matrices.

In Figs. 1 and 2 we show the optical phonon dispersions, $\omega(q)$, of MoX₂ and WX₂ (X=S, Se, Te) for phonon wave vectors $q \leq 0.25(2\pi/a)$. The six optical branches ZO₁, ZO₂, LO₂, TO₂, LO₁, and TO₁ along the $\Gamma \rightarrow K$ direction of the BZ obtained by the *ab initio* procedure are shown by straight lines, while the data from the phenomenological continuous approach are represented by dots. The values of all the parameters employed to evaluate $\omega(q)$ are listed in Table I. To obtain the polarizability, α_2 from Eq. (16), we follow the procedure of Ref. [19] where for an isolated TMD the screening

TABLE I. Employed parameters for the evaluation of the out-plane and in-plane dispersion relations as give by Eqs. (16), (17), (22), (25), (26), and (28). a is optimized lattice constant, c is interlayer distance, d is thickness of the monolayer, $r_0 = 2\pi\alpha_2$ is the screening parameter, and ϵ is dielectric constant.

	MoS ₂	MoSe ₂	MoTe ₂	WS ₂	WSe ₂	WTe ₂
a (Å)	3.1635	3.2974	3.5274	3.1627	3.2954	3.5296
c (Å)	15.9300	16.4871	17.6370	15.8137	16.4772	17.6481
r_0 (Å)	46.0182	53.3517	68.6562	41.8979	48.7041	64.8081
d (Å)	5.4817	5.9712	6.6789	5.5093	6.0065	6.6978
ϵ	16.8096	17.9009	20.5752	15.2536	16.2581	19.3865

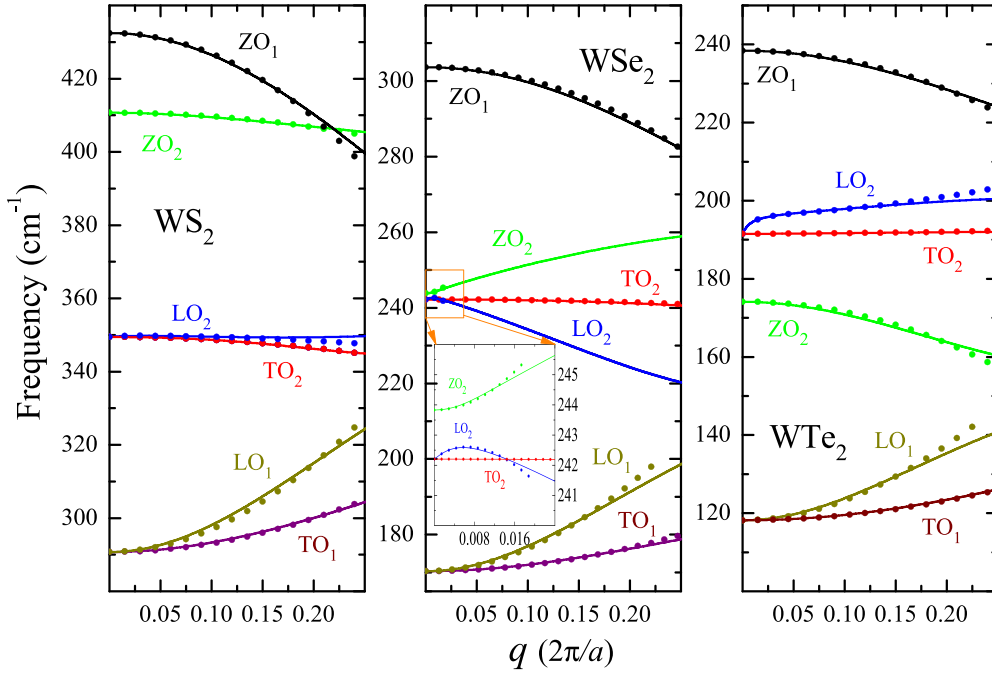


FIG. 2. The same as Fig. 1 for 1M WX_2 ($X=S, Se, Te$). The inset shows the phonon dispersion of $ZO_2, LO_2,$ and TO_2 in the small momenta interval for WSe_2 .

parameter $r_0 = 2\pi\alpha_2$ is reduced to

$$r_0 = \left(\frac{\epsilon}{2} - \frac{1}{3\epsilon} \right) d, \quad (29)$$

with the dielectric constant ϵ evaluated using the standard 3D QE code [19]. In both figures we notice the well known trend of the phonon frequency with the reduced mass, $\omega \sim \sqrt{1/\mu}$, i.e., as μ increases the optical phonon frequency decreases. The most notable example is the out-of-plane ZO_2 mode (green lines and dots in the figures), for this mode $\mu = m_x/2$. Good agreement between the first-principles and phenomenological model calculations is achieved for the phonon dispersions covering up to 20% or higher around the Γ point of the BZ. For the MoS_2 the LO_2 branch presents an agreement lower than 16%. The exceptions are the ZO_2 and LO_2 modes of WSe_2 where we achieve a concordance smaller than 2%; we discuss this behavior in Sec. IV.

IV. PARAMETERS OF THE MODEL FROM *AB INITIO* CALCULATIONS

We are able to extract the characteristic parameters of the phonon frequencies $\omega = \omega(q; \alpha, \beta_1, \beta_2)$ for each phonon symmetry $A_2, A_1, E',$ and E'' at Γ by fitting the phonon dispersion laws obtained from *ab initio* calculations to the equations proposed in our phenomenological model. These sets of parameters provide a simple description of the phonon dispersion curves, LO_2 - TO_2 splitting, as well as for electron-phonon interaction. For the fitting procedure we introduce the dimensionless curvature parameters $C_\delta = \pm(2\pi\beta_\delta)^2/(a\omega_\delta)^2$ and the dimensionless slope $\Xi = (2\pi\alpha)^2/(a\rho_m\omega_{E'}^2)$, where $\delta = A_2(ZO_1), A_1(ZO_2), E'(LO_2, TO_2),$ and $E''(LO_1, TO_1)$ account for the phonon symmetry. Employing the analytical phonon dispersions detailed in Eqs. (16), (17), (22), (25),

(26), (28) and those provided by first principle calculations along the $\Gamma \rightarrow K$ direction; in Table II we collect the relevant parameters of the six optical phonon branches. For phonon wave vectors $q \leq 0.25(2\pi/a)$ the two independent directions $\Gamma \rightarrow K$ and $\Gamma \rightarrow M$ provide practically the same values for both coefficients Ξ and C_δ .

A. LO_2 - TO_2 splitting

An important result valid for resonant Raman scattering [31], transport effects [9], polaron effects [32],

TABLE II. Phonons data of $MoS_2, MoSe_2, MoTe_2, WS_2, WSe_2,$ and WTe_2 of 1M TMDs. The dimensionless curvature $C_\delta = \pm(2\pi\beta_\delta)^2/(a\omega_\delta)^2$ and the dimensionless slope $\Xi = (2\pi\alpha)^2/(a\rho_m\omega_{E'}^2)$ are estimated from the dispersions curves $\omega(q)$ [see Eqs. (16), (17), (22), (25), (26), and (28)] and the phonon dispersion law obtained by *ab initio* calculations for the six optical branches $\delta = A_2(ZO_1), A_1(ZO_2), E'(LO_2, TO_2),$ and $E''(LO_1, TO_1)$. ω_δ in cm^{-1} .

	MoS_2	$MoSe_2$	$MoTe_2$	WS_2	WSe_2	WTe_2
ω_{A_2}	463.73	347.97	289.03	432.45	303.65	238.41
C_{ZO_1}	-2.38	-1.95	-1.62.	-2.6.	-2.2	-2.05
ω_{A_1}	399.29	236.83	170.26	410.69	243.83	174.12
C_{ZO_2}	0.78	-2.68	-2.25	-0.48	41	-2.95
$\omega_{E'}$	378.10	280.96	233.20	349.44	242.20	191.53
C_{LO_2}	-2.85	0.54	-0.60	-0.22	-36.5	1.1
Ξ	1.03	3.3	12	0.23	1.2	7.0
C_{TO_2}	0.46	0.23	0.52	-0.43	-0.16	0.13
$\omega_{E''}$	279.51	164.34	115.80	290.73	170.31	118.18
C_{LO_1}	4.7	7.45	9.84	4.3	7.2	8.8
C_{TO_1}	1.39	1.61	2.12	1.6	1.84	2.17

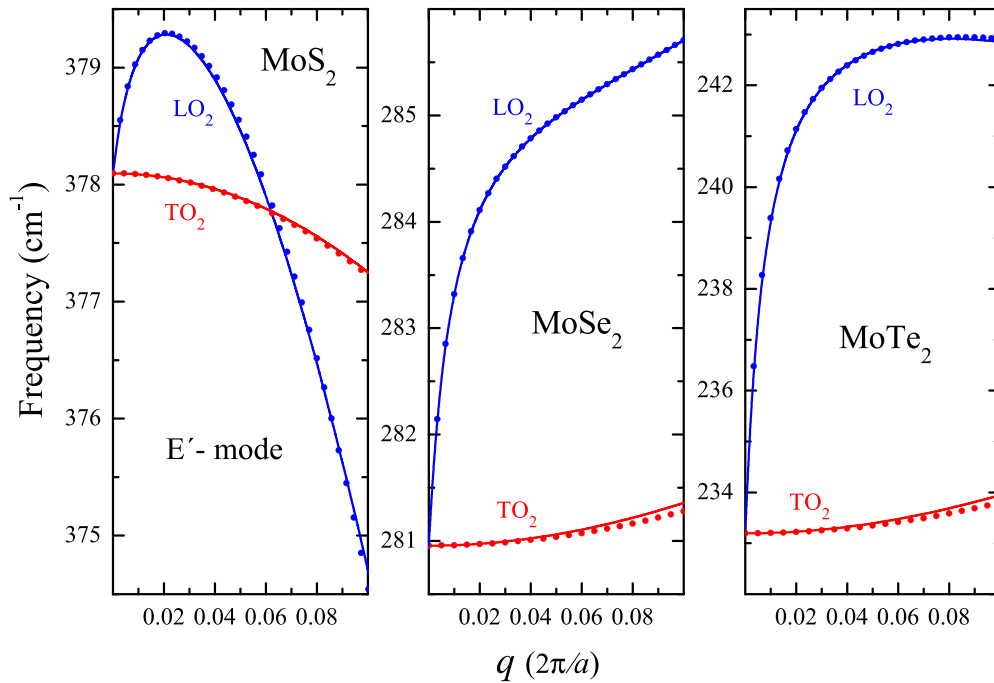


FIG. 3. LO₂-TO₂ splitting for 1M MoX₂ (X=S, Se, Te). LO₂ (blue) and TO₂ (red) optical modes. Straight lines correspond to *ab initio* calculations; dots represent the dispersion laws obtained by Eqs. (16) and (17).

magneto-polaron [33], exciton-phonon resonances [34], and magneto-Raman scattering [35] among other properties is the splitting between the longitudinal and transverse optical modes. Using the analytical results for the phonon dispersion law we can study the $\hbar\omega_{\text{LO}_2} - \hbar\omega_{\text{TO}_2}$ energy splitting and its dependence on the characteristic parameters of the material under consideration. Figures 3 and 4 show the dependence of the frequencies ω_{LO_2} and ω_{TO_2} on q for the series of MoX₂

and WX₂ TMD materials. We observe an excellent agreement of Eqs. (16) and (17) with our first-principle calculations. In addition, it is clearly seen the linear dispersion relation of the LO₂ modes for $1 \gg 2\pi\alpha_2q$ and for the WSe₂ the long wave phenomenological model, as dictated by Eq. (1), provides good results for the LO₂ branch if $q < 0.016 \times 2\pi/a$. From the analytical results displayed in Sec. II A we can extract several conclusions. Using Eqs. (16) and (17) the energy of

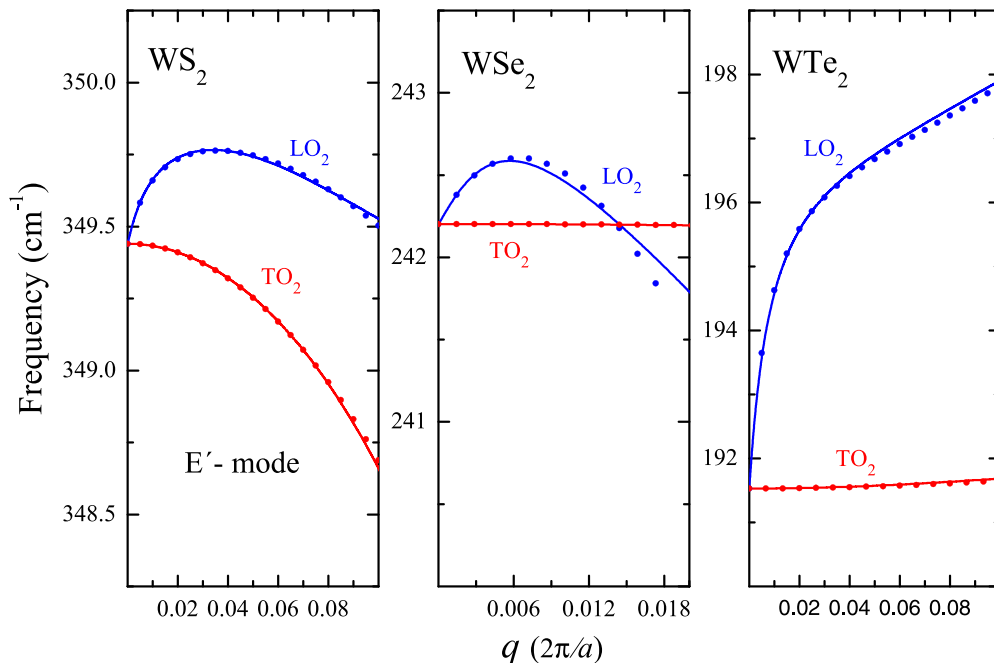


FIG. 4. The same as Fig. 3 for WX₂ (X=S, Se, Te).

TABLE III. Comparison of the LO₂-TO₂ splitting coefficients S_{Ph} and S reported in Ref. [36] for several TMDs.

	MoS ₂	MoSe ₂	MoTe ₂	WS ₂	WSe ₂	WTe ₂
S (10^{-3} eV ² Å)	1.13	2.09	4.87	0.21	0.625	
S_{Ph} (10^{-3} eV ² Å)	1.14	2.10	5.63	0.22	0.568	2.21

the LO₂-TO₂ splitting is given by

$$\begin{aligned} \Delta E_{LO_2-TO_2}^2 &= \hbar^2 \omega_{LO_2}^2 - \hbar^2 \omega_{TO_2}^2 \\ &= S_{Ph} \frac{q}{(1 + 2\pi\alpha_2 q)} + \hbar^2 \Delta\beta^2 q^2, \end{aligned} \quad (30)$$

with the coefficient $S_{Ph} = 2\pi(\hbar\alpha)^2/\rho_m$ and $\Delta\beta^2 = \pm\beta_{LO_2}^2 \mp \beta_{TO_2}^2$. Equation (30) shows that for $q \rightarrow 0$, $\Delta E_{LO_2-TO_2} = \hbar\omega_{LO_2} - \hbar\omega_{TO_2}$ is linear on q with a slope $P = S_{Ph}/2\hbar\omega_{E'}$. A similar expression has been obtained in Ref. [18] from a microscopic dipole lattice model and Ref. [36] by first-principles calculations, respectively. In Table III we compare the LO₂-TO₂ splitting coefficients S_{Ph} obtained from Eq. (30) and S from Ref. [36]. Notice that Eq. (30) predicts that $\Delta E_{LO_2-TO_2}$ has a maximum in the neighborhood of $q \sim 0$ for such systems with negative curvature, i.e., $\mathbb{C}_{LO_2} < 0$ and $\beta_{LO_2}^2 > \beta_{TO_2}^2$ in the phonon dispersion law (MoS₂ and WSe₂). Hence, the LO₂-TO₂ splitting may present a maximum at certain $q = q_0 > 0$ solutions of the equation

$$q_0(1 + r_0 q_0)^2 = -\frac{S_{Ph}}{2\hbar^2 \Delta\beta^2}. \quad (31)$$

Hence, we learn that as the curvature β_{LO_2} increases $q_0 \rightarrow 0$. As a consequence, the maximum value of the function $\Delta E_{LO_2-TO_2}(q_0)$ decreases, explaining those results for the LO₂-TO₂ splitting of MoS₂ and WSe₂ as shown in Figs. 3 and 4. Moreover, if the transverse curvature \mathbb{C}_{TO_2} is negative and the TO₂-phonon dispersion cannot be considered flat, the LO₂-phonon dispersion, Eq. (16), has a maximum at $q = q_0$ solution of Eq. (31). This is the case of the WS₂ shown in Fig. 4. It is important to keep in mind that the inclusion of quadratic terms in the equation of motion, proportional to phenomenological parameters $\beta_{LO_2}^2$ and $\beta_{TO_2}^2$, is responsible for the correct description of the $\omega_{LO_2}(q)$ phonon law. From Table III it follows that for each series of MX₂ (X = S, Se, Te), $\Delta E_{LO_2-TO_2}^2$ increases as we move from S to Te. To explain the dependence of $\Delta E_{LO_2-TO_2}^2$ on chalcogen ions, we realize that the force constant values \mathbb{F}_X employed in the first-principle calculations meet the inequality $\mathbb{F}_{Te} < \mathbb{F}_{Se} < \mathbb{F}_S$. Therefore, for smaller values of \mathbb{F}_X we get larger LO₂-TO₂ splitting. In addition, if we compare the slopes of the MoX₂ set with those of WX₂, we find that the Mo compounds have a splitting coefficient S_{Ph} greater than the W counterparts.

V. ELECTRON-PHONON INTERACTION IN 2D TMD SEMICONDUCTORS

The intravalley electron scattering processes in TMD are associated with two main mechanisms: Fröhlich and deformation potential. The first one is linked to internal electrical

polarization associated to the optical vibration \mathbf{u} . The LO₂-phonon lattice vibration in the TMD layer gives rise to a 2D macroscopic electric field that couples to the charge carriers in the same band. The second is due to the dispersive mechanical nature. The A₁ phonon, with the metal atom fixed and the chalcogen atoms vibrating in phase opposition out of plane, is also associated to intraband transitions of carriers. It is mandatory in studies of transport properties [37], mobility [38], carriers relaxation time [11], scattering of photoexcited carriers [10], optoelectronic functionality [39], photonic [40], and resonant Raman scattering in external fields [41], to know the relative contributions of both interactions. The relative importance of the Pekar-Fröhlich and the deformation potential interactions depend on the material and the band (conduction or valence) under consideration [19].

Recently, the authors of Ref. [42] were able to resolve the spectral characteristics of the phonon sidebands by using a 2D microspectroscopy. The method is very promising for measuring exciton-phonon coupling in monolayers of TMDs. Surprisingly, in the case of 1ML MoSe₂ a Huang-Rhys factor of the order of 1 is obtained, a rather high value compared to polar II-VI semiconductors. Furthermore, Ref. [43] addresses the influence of the electron-phonon coupling on the electronic transport properties of 1ML 2H-TaS₂ monolayer, a new 2D compound where the phonon modes have the same symmetry properties as 1ML TMDs studied here.

In this section we present detailed calculations of the Pekar-Fröhlich and deformation potential electron-phonon Hamiltonians.

A. Pekar-Fröhlich-type Hamiltonian

The Pekar-Fröhlich Hamiltonian H_F is proportional to the LO₂-TO₂ phonon splitting which is ruled by the coupling constant α . This parameter determines the strength of the electron-phonon interaction. For TMD materials, H_F can be written as

$$H_F = -e\varphi_2(\boldsymbol{\rho}). \quad (32)$$

Using Eq. (13) we obtain [23]

$$\varphi_2 = -\frac{\alpha}{2\pi} \int \frac{F(\mathbf{q})}{q(1 + 2\pi\alpha_2 q)} e^{i\mathbf{q}\cdot\boldsymbol{\rho}} d^2 q, \quad (33)$$

with $F(\mathbf{q})$ given by Eq. (14). The general canonical quantum-mechanical version for the LO₂-vibrational amplitude can be cast as [23]

$$\hat{\mathbf{u}}_{E'} = \sum_{\mathbf{q}} \frac{\mathbf{q}}{q} \left(\frac{\hbar}{2\rho_m N_c A \omega_{E'}} \right)^{1/2} [\hat{b}_{\mathbf{q}} e^{i\mathbf{q}\cdot\boldsymbol{\rho}} + \hat{b}_{\mathbf{q}}^\dagger e^{-i\mathbf{q}\cdot\boldsymbol{\rho}}], \quad (34)$$

where $\omega_{E'}$ is the phonon frequency in Eq. (16), A the area of the unit cell, N_c the number of cells, and $\hat{b}_{\mathbf{q}}^\dagger$ ($\hat{b}_{\mathbf{q}}$) the creation (annihilation) phonon operator. Inserting Eq. (34) into Eqs. (14) and (33) we finally obtain

$$H_F = -i \sum_{\mathbf{q}} \frac{\mathbb{G}_{Ph}}{\sqrt{N_c}(1 + r_0 q)} [\hat{b}_{\mathbf{q}} e^{i\mathbf{q}\cdot\boldsymbol{\rho}} + \hat{b}_{\mathbf{q}}^\dagger e^{-i\mathbf{q}\cdot\boldsymbol{\rho}}], \quad (35)$$

TABLE IV. Comparison of the Fröhlich constants \mathbb{G}_{Ph} from Eq. (36) following the fitting procedure \mathbb{G}_F considering our *ab initio* calculations as given by Eq. (37) and those reported in Ref. [19] for several 1ML TMDs.

Material	MoS ₂	MoSe ₂	MoTe ₂	WS ₂	WSe ₂	WTe ₂
\mathbb{G}_{Ph} (eV)	0.356	0.538	0.904	0.162	0.301	0.625
\mathbb{G}_F (eV)	0.352	0.531	0.858	0.163	0.309	0.592
\mathbb{G}_{ab} (eV)	0.334	0.502	0.819	0.140	0.276	

where

$$\mathbb{G}_{Ph} = \left(\frac{2\pi^2 e^2 \hbar \alpha^2}{A \rho_m \omega_{E'}} \right)^{1/2} \quad (36)$$

is the Fröhlich coupling constant obtained by the fitting procedure of the parameter α and the LO₂-phonon dispersion. In addition, the Fröhlich interaction can be cast in terms of the Born effective charges as given by [19,44]

$$\mathbb{G}_F = \frac{2\pi e^2}{A} \sum_i \frac{\mathbf{e}\mathbf{q} \cdot \mathbb{Z}_i \cdot \mathbf{e}_{LO}}{\sqrt{2M_i \omega_q}}, \quad (37)$$

where M_i is the mass of atom i , \mathbb{Z}_i the tensors of Born effective charge, $\mathbf{e}\mathbf{q}$ the unit vector along the \mathbf{q} vector, and \mathbf{e}_{LO} the eigenvector of the LO₂ phonon. In Table IV we compare the Fröhlich constants \mathbb{G}_{Ph} and \mathbb{G}_F from Eqs. (36) and (37), respectively, with those values reported in Ref. [19], \mathbb{G}_{ab} , for several TMD materials. The small differences between the values of \mathbb{G}_F and \mathbb{G}_{ab} should be awarded to force constants employed in the first principle calculations.

B. Deformation potential interaction

Optical homopolar mode changes the electronic energy band due to the mechanical deformation of the atoms in the primitive unit cell. This coupling is known as deformation potential and, in the first order of approximation, we will consider this interaction independent of the phonon wave vector. The first-order deformation potential in \mathbf{q} accounts for electronic intervalley transitions assisted by the ZO₂ modes. Assuming the Born-Oppenheimer approximation the electron-phonon contribution to the electronic Hamiltonian of the crystal, H_c , is defined as [45]

$$H_{Dp} = \sum_l \left(\frac{\partial H_c}{\partial \mathbf{R}_l} \right) \Big|_0 \cdot \delta \mathbf{R}_l, \quad (38)$$

where $\delta \mathbf{R}_l$ is the atom displacements from the equilibrium. In the long-wavelength limit, the homopolar phonon can be considered as microscopic oscillation within the primitive cell independent of the phonon wave vector \mathbf{q} and $\delta \mathbf{R}_l \approx \mathbf{u}_{z_{O_2}}$ the relative vector displacement out of plane for the A₁(ZO₂) mode (see Sec II B). Considering a nondegenerate band with energy $E_{\mathbf{k}}$, Eq. (38) is reduced to

$$H_{Dp} = D_p \mathbf{e}_z \cdot \mathbf{u}_{z_{O_2}}, \quad (39)$$

where D_p is the deformation potential characterizing the changes of the electronic energy for \mathbf{k} near the K point of the BZ due to the phonon lattice oscillation $\mathbf{u}_{z_{O_2}}$. Writing $\mathbf{u}_{z_{O_2}}$ in

terms of creation and annihilation phonon operators we have

$$H_{Dp} = \sum_{\mathbf{q}} D_p \left(\frac{\hbar}{2\rho_m N_c A \omega_{O_{A_1}}} \right)^{1/2} [\hat{b}_{\mathbf{q}} e^{i\mathbf{q}\cdot\rho} + \hat{b}_{\mathbf{q}}^\dagger e^{-i\mathbf{q}\cdot\rho}], \quad (40)$$

with $\omega_{O_{A_1}}$ the ZO₂-phonon frequency (28).

It becomes clear that the electron-phonon coupling in Eq. (40) is independent of the phonon wave vector, and it corresponds to short-range interaction. As a consequence, H_{Dp} is responsible for the intravalley transitions coupling electrons (holes) in the lowest (upper) nondegenerate conduction (valence) band. The values of the optical-phonon deformation potentials can be extracted by Raman scattering technique [45], transport properties [37], tight-binding [46], or first-principle calculations [8].

VI. POLARON PROPERTIES: EFFECTIVE MASS AND BINDING ENERGY

Polaron effects are particularly interesting for cyclotron resonance experiments [47], magneto-polaron resonances [33,48], and magneto-Raman scattering [49]. The authors in Ref. [50] discussed the role of the polaron effect in the absorption spectra of TMDs. Theoretical evaluations show an asymmetric phonon sideband and polaron redshift in the optical absorption spectra in good agreement with the experimental observation of 1ML MoSe₂, MoS₂, WSe₂, and WS₂. In 3D semiconductors the binding energy and effective mass depend strongly on the coupling of electrons with LO phonons at small momenta. The polaron correction in quasi-2D systems as quantum wells is a good example as the dimensionality affects the electron-optical phonon coupling [51]. A straightforward application of the electron-phonon Hamiltonians for 2D TMD developed in Sec. V is the evaluation of the polaron energy of electrons at the K valley. Employing the general Green's function formalism, the polaron state is obtained by solving the Dyson equation [52]

$$G(\mathbf{k}) = G^{(0)}(\mathbf{k}) + G^{(0)}(\mathbf{k}) \sum_{\mathbf{k}', \mathbf{q}} S_{\mathbf{k}, \mathbf{k}'}(\mathbf{q}) G(\mathbf{k}'), \quad (41)$$

where $G(\mathbf{k})$ ($G^{(0)}$) is the $T = 0$ K one-particle Green's function (unperturbed) for the electron and $S_{\mathbf{k}, \mathbf{k}'}(\mathbf{q})$ the irreducible self-energy. For the unperturbed Green function we know that

$$G^{(0)} = \frac{1}{\varepsilon - \frac{\hbar^2 k^2}{2m} + i\delta_0}, \quad (42)$$

with m the electron effective mass and $\delta_0 \rightarrow 0$. To lowest order of electron-optical phonon interaction $S_{\mathbf{k}, \mathbf{k}'}(\mathbf{q}) = S(\mathbf{k}, \mathbf{q}) \delta_{\mathbf{k}, \mathbf{k}'+\mathbf{q}}$, thus, solving Eq. (41) we obtain that

$$G(\mathbf{k}) = \frac{1}{\varepsilon - \frac{\hbar^2 k^2}{2m} - S_\varepsilon(\mathbf{k}) + i\delta_1}, \quad (43)$$

with S_ε the self-energy as given by

$$S_\varepsilon = \sum_{\mathbf{q}} \frac{|C_q|^2}{\frac{\hbar^2}{2m} [k^2 - |\mathbf{k} - \mathbf{q}|^2] - \hbar\omega_0 + i\delta_1}, \quad (44)$$

TABLE V. Polaron mass m_p , binding energy $\Delta\varepsilon_p$, the Fröhlich $2\alpha_F f_3(R_0)$, and deformation potential $\alpha_{Dp}/4$ contributions for several 1ML TMD. m is the electron effective mass at the K point, m_0 the bare electron mass, and D_p the deformation potential.

Material	MoS ₂	MoSe ₂	MoTe ₂	WS ₂	WSe ₂
m/m_0	0.51 ^a	0.64 ^a	0.56 ^b	0.31 ^a	0.39 ^a
D_p (eV/Å)	5.8 ^a	5.2 ^a	1.34 ^c	3.1 ^a	2.3 ^a
$2\alpha_F f_3(R_0)$	0.009	0.032	0.094	0.002	0.013
$\alpha_{Dp}/4$	0.017	0.035	0.004	0.002	0.003
m_p/m_0	1.027	1.071	1.108	1.004	1.016
$\Delta\varepsilon_p$ (eV)	-0.0024	-0.0028	-0.0002	-0.0003	-0.0003

^aRef. [37]

^bRef. [19]

^cRef. [38]

C_q being the coupling constant, ω_0 the optical-phonon frequency, and the parameter $\delta_1 \rightarrow 0$. For the evaluation of the renormalized energy spectrum for conduction electrons, $\varepsilon(\mathbf{k})$, we take the real part of $G(\mathbf{k})$. Considering 3D bulk semiconductors the polaron effective mass and polaron binding energy are $m_{3D} = m/(1 - \alpha_{3D}/6)$ and $\Delta\varepsilon = -\alpha_{3D}\hbar\omega_{LO}$, respectively, with α_{3D} the Fröhlich coupling constant and ω_{LO} the LO phonon frequency [53].

In 2D TMDs the LO₂ and A₁(ZO₂) modes couple to the lower (upper) conduction (valence) band. In consequence, to evaluate the self-energy (44) we have to add the short-range deformation potential interaction (40) to the typical Pekar-Fröhlich contribution (35). It is possible to show that the polaron effective mass and binding energy are given by (see Appendix B)

$$m_p = \frac{m}{1 - \alpha_p}, \quad \Delta\varepsilon_p = -\alpha_F \hbar\omega_{E'} f_1(R_0) - \alpha_{Dp} \hbar\omega_{0A_1} \ln 2, \quad (45)$$

with $\alpha_p = 2\alpha_F f_3(R_0) + \alpha_{Dp}/4$. The function $f_i(R_0)$ ($i = 1, 3$) and the effective coupling constant α_F and α_{Dp} are detailed in the Appendix B. The values of m_p/m_0 and $\Delta\varepsilon_p$ are summarized in Table V for the TMD family; for the evaluation we employ the parameters of Tables II and IV.

From the results of Table V we have that for a given series of MX₂ compounds as the mass of the chalcogen atom X increases, the m_p increases following the same trend of the Fröhlich coupling constant (36). In addition, it can be seen that the deformation potential plays a crucial role in the binding energy and in the polaron mass, in particular, of the MoS₂ and MoSe₂ monolayers. For the WX₂ compounds the deformation potential contribution is weaker than MoX₂ ones.

VII. CONCLUSIONS

We implemented a continuum phenomenological approach valid for any monolayer TMDs family. The model accurately describes the dispersive phonon spectra of the nonpolar and polar optical phonon modes with in-plane (LO₁, TO₁, LO₂, and TO₂) or out-of-plane oscillations (ZO₁ and ZO₂). We employed *ab initio* calculations to evaluate the characteristic parameters of the phonon dispersion laws up to parabolic term with the wave vector. These results allow us to establish the validity of our macroscopic phenomenological approach

(see Figs. 1–4). The compiled data in Table II for the description of the six optical phonon modes and the long-range electron-phonon strength interaction for the 1ML TMD family constitutes one of the main results of the present work.

Under the condition that the curvature parameters of the TMD meet the inequality $\beta_{LO_2} > \beta_{TO_2}$, we predict that the LO₂-TO₂ splitting has a maximum for TMDs with negative curvature in the phonon dispersion. For the case of LO₂ and ZO₂ oscillations in WSe₂, the range of validity of their respective phonon dispersions is restricted to a small interval of q ($q < 0.016 2\pi/a$ in Fig. 2). A plausible explanation is that our model in (1) does not take into account the interplay between A₁ and E' phonon. The frequency separation between ω_{0A_1} and $\omega_{E'}$ is less than 2 cm⁻¹.

The present results provide a complete description of the 2D long-range (35) and short-range homopolar deformation potential (40) electron-phonon interactions. We report in Table IV the values of the coupling constant needed to obtain analytically the 2D intravalley Pekar-Fröhlich Hamiltonian for the TMDs family. Finally, using the electron-phonon Hamiltonians (35) and (40) we report the polaron properties for TMDs MoS₂, MoSe₂, MoTe₂, WS₂, and WSe₂. Consequently, the results detailed in Table V show that the contribution of the deformation-potential interaction associated with the A₁ mode cannot be disregarded. This conclusion is valid for all those processes involving the evaluation of the electron or hole intraband transitions (mobility, scattering rate, Raman dispersion, among others) assisted by the electron-optical phonon interaction.

Last but not least, it is important to note that the model developed here could be extended to other 2D TMD families [54]. However, the extension of our phenomenological model is not a straightforward task. For instance, in monolayers of 1T-TaX₂ phase, the symmetry of the unit cell is different than the 2H phase we studied [43]. On the contrary, in the 1ML 2H-TaSe₂ phase, the optical modes at Γ show the same vibrational and symmetry properties as those TMDs here analyzed [55]. The phenomenological model can be extended to this system and the equations of motion (1) and (23) are valid to describe the six optical branches.

ACKNOWLEDGMENTS

R.P.-A. thanks CONACyT/Mexico for a sabbatical Grant. E.S.M and E.M.-P. acknowledge support by FONDECYT Chile Grant No. 1170921.

APPENDIX A: “STRESS” TENSOR AND DISPERSIVE OSCILLATIONS

In order to account for dispersion oscillations of the phonons along a given direction of the BZ, we introduce the tensor $\vec{\sigma}$ in Eq. (1). This tensor can be associated to some kind of internal “stress” and considering the similarity with the elastic theory [56,57] we define $\vec{\sigma}$ as

$$\vec{\sigma} = \vec{\vec{C}} : \nabla U(\rho), \quad (A1)$$

where $\vec{\vec{C}}$ plays the same role of the “elastic constant” or the “elastic stiffness” tensor [21]. The fourth rank tensor $\vec{\vec{C}}$ must have the same symmetry properties of the elastic constant of

the medium. For the 2D TMD structure with a D_{3h} symmetry we have to deal with five independent parameters and $\vec{\sigma}$ can be cast as

$$\begin{pmatrix} \sigma_{xx} \\ \sigma_{yy} \\ \sigma_{zz} \\ \sigma_{zx} \\ \sigma_{yz} \\ \sigma_{xy} \end{pmatrix} = \rho_m \begin{pmatrix} \beta_{11}^2 & \beta_{12}^2 & \beta_{13}^2 & 0 & 0 & 0 \\ \beta_{12}^2 & \beta_{11}^2 & \beta_{13}^2 & 0 & 0 & 0 \\ \beta_{13}^2 & \beta_{13}^2 & \beta_{33}^2 & 0 & 0 & 0 \\ 0 & 0 & 0 & \beta_{44}^2 & 0 & 0 \\ 0 & 0 & 0 & 0 & \beta_{44}^2 & 0 \\ 0 & 0 & 0 & 0 & 0 & \frac{1}{2}(\beta_{11}^2 - \beta_{12}^2) \end{pmatrix} \times \begin{pmatrix} U_{xx} \\ U_{yy} \\ U_{zz} \\ 2U_{zx} \\ 2U_{yz} \\ 2U_{xy} \end{pmatrix}, \quad (\text{A2})$$

with $U_{ij} = \frac{1}{2}(\partial_i U_j + \partial_j U_i)$. For the case of 1ML TMD where we assume strictly a 2D system, the terms $\partial_z U_i = 0$ ($i = x, y, z$). Taking the parameters $\beta_{11}^2 = \beta_{\text{Lo}_2}^2$, $\frac{1}{2}(\beta_{11}^2 - \beta_{12}^2) = \beta_{\text{To}_2}^2$ and $\beta_{44}^2 = \beta_{\text{zo}_1}^2$ immediately follows Eq. (4).

APPENDIX B: POLARON PROPERTIES

The total self-energy $S_\varepsilon = S_\varepsilon^{(F)} + S_\varepsilon^{(Dp)}$ where $S_\varepsilon^{(F)}$ corresponds to the Fröhlich interaction while $S_\varepsilon^{(Dp)}$ to the mechanical lattice distortion.

1. Fröhlich contribution

From Eq. (35) it follows that $C_q = \mathbb{G}_{Ph}/\sqrt{N_c}(1 + r_0q)$. Thus, the self-energy $S_\varepsilon^{(F)}$ can be written as

$$S_\varepsilon^{(F)} = -\alpha_F \hbar \omega_{E'} F(\kappa, R_0), \quad (\text{B1})$$

where $\kappa = k/\sqrt{\hbar/2m\omega_{E'}}$, $R_0 = r_0\sqrt{2m\omega_{E'}/\hbar}$,

$$\alpha_F = \frac{\sqrt{3}}{2\pi} \frac{m}{\hbar^2 a^{-2}} \frac{\mathbb{G}_{Ph}^2}{\hbar \omega_{E'}}, \quad (\text{B2})$$

and

$$F(\kappa, R_0) = \int_0^\infty \frac{z}{(1 + R_0 z)^2 \sqrt{(1 + z^2)^2 - 4\kappa^2 z^2}} dz. \quad (\text{B3})$$

If $\hbar^2 k^2/(2m) < \hbar \omega_{E'}$ we can approximate the function

$$(1 + z^2 - 4\kappa^2 z^2)^{-1/2} \approx \frac{1}{z^2 + 1} + \frac{2z^2}{(z^2 + 1)^3} \kappa^2, \quad (\text{B4})$$

and $S_\varepsilon^{(F)}$ can be cast as

$$S_\varepsilon^{(F)} = -\alpha_F \hbar \omega_{E'} [f_1(R_0) + 2\kappa^2 f_3(R_0)], \quad (\text{B5})$$

with

$$f_p = \int_0^\infty \frac{z^p}{(1 + R_0 z)^2 (1 + z^2)^p} dz. \quad (\text{B6})$$

2. Deformation potential

For the A_1 modes the electron-deformation potential coupling constant is

$$C_q^2 = \frac{\hbar}{2\rho_m N_c A \omega_{0A_1}} D_p^2 \quad (\text{B7})$$

and for the $S_\varepsilon^{(Dp)}$ we obtain

$$S_\varepsilon^{(Dp)} = -\alpha_{Dp} \hbar \omega_{0A_1} \left[\ln 2 + \frac{\kappa^2}{4} \right], \quad (\text{B8})$$

where

$$\alpha_{Dp} = \frac{m}{4\pi \rho_m} \left(\frac{D_p}{\hbar \omega_{0A_1}} \right)^2. \quad (\text{B9})$$

Taking the real part of the Green function (43) we obtain the 2D polaron energy as

$$\varepsilon_p(\mathbf{k}) = \frac{\hbar^2 k^2}{2m} \left[1 - 2\alpha_F f_3(R_0) + \frac{\alpha_{Dp}}{4} \right] - \alpha_F \hbar \omega_{E'} f_1(R_0) - \alpha_{Dp} \hbar \omega_{0A_1} \ln 2. \quad (\text{B10})$$

-
- [1] T. C. Berkelbach and D. R. Reichman, *Annu. Rev. Condens. Matter Phys.* **9**, 379 (2018).
- [2] S. Anju, P. V. Mohanan, X. Zhang, S. Y. Teng, A. C. M. Loy, B. S. How, W. D. Leong, and X. Tao, *Nanomaterials* **10**, 1012 (2020).
- [3] K. Khan, A. Khan Tareen, M. Aslam, R. Wang, Y. Zhang, A. Mahmood, Zh. Ouyang, H. Zhang, and Z. Guo, *J. Mater. Chem. C* **8**, 387 (2020).
- [4] G. Fiori, F. Bonaccorso, G. Iannaccone, T. Palacios, D. Neumaier, A. Seabaugh, S. K. Banerjee, and L. Colombo, *Nat. Nanotechnol.* **9**, 768 (2014); D. Jariwala, V. K. Sangwan, L. J. Lauhon, T. J. Marks, and M. Hersam, *ACS Nano*. **8**, 1102 (2014).
- [5] H. Zenga and X. Cui, *Chem. Soc. Rev.* **44**, 2629 (2015).
- [6] B. Radisavljevic, A. Radenovic, J. Brivio *et al.*, *Nat. Nanotechnol.* **6**, 147 (2011).
- [7] Y. Song and H. Dery, *Phys. Rev. Lett.* **111**, 026601 (2013).
- [8] K. Kaasbjerg, K. S. Thygesen, and K. W. Jacobsen, *Phys. Rev. B* **85**, 115317 (2012).
- [9] X. Li, J. T. Mullen, Z. Jin, K. M. Borysenko, M. Buongiorno Nardelli, and K. W. Kim, *Phys. Rev. B* **87**, 115418 (2013).
- [10] M. Danovich, I. L. Aleiner, N. D. Drummond, and V. I. Fal'kov, *IEEE J. Quantum Electron.* **23**, 168 (2017).
- [11] I. Paradisanos, G. Wang, E. M. Alexeev, A. R. Cadore, X. Marie, A. C. Ferrari, M. M. Glazov, and B. Urbaszek, *Nat. Commun.* **12**, 538 (2021).
- [12] H. Zhu, Y. Wang, J. Xiao, M. Liu, Sh. Xiong, Z. J. Wong, Z. Ye, Y. Ye, X. Yin, and X. Zhang, *Nat. Nanotechnol.* **10**, 151 (2014).
- [13] S. Brem, A. Ekman, D. Christiansen, F. Katsch, M. Selig, C. Robert, X. Marie, B. Urbaszek, A. Knorr, and E. Malic, *Nano Lett.* **20**, 2849 (2020).

- [14] N. A. Pike, A. Dewandre, B. Van Troeye, X. Gonze, and M. J. Verstraete, *Phys. Rev. Material* **3**, 074009 (2019).
- [15] J. Ribeiro-Soares, R. M. Almeida, E. B. Barros, P. T. Araujo, M. S. Dresselhaus, L. G. Cancado, and A. Jorio, *Phys. Rev. B* **90**, 115438 (2014).
- [16] X. Zhang, X.-F. Qiao, W. Shi, J.-B. Wu, De-S. Jiang, and P.-H. Tan, *Chem. Soc. Rev.* **44**, 2757 (2015).
- [17] A. Molina-Sánchez and L. Wirtz, *Phys. Rev. B* **84**, 155413 (2011).
- [18] J.-Z. Zhang, *AIP Adv.* **10**, 045316 (2020).
- [19] Th. Sohier, M. Calandra, and F. Mauri, *Phys. Rev. B* **94**, 085415 (2016).
- [20] P. Cudazzo, I. V. Tokatly, and A. Rubio, *Phys. Rev. B* **84**, 085406 (2011).
- [21] C. Trallero-Giner and F. Comas, *Phys. Rev. B* **37**, 4583 (1988); *Philos. Mag. B* **70**, 583 (1994); C. Trallero-Giner, R. Pérez-Álvarez, and F. García-Moliner, *Long Wave Polar Optical Modes in Semiconductor Heterostructures* (Pergamon, London, 1998).
- [22] M. Born and K. Huang, *Dynamical Theory of Crystal Lattice* (Clarendon Press, Oxford, 1988).
- [23] C. Trallero-Giner, E. Menéndez-Proupin, E. Suárez Morell, R. Pérez-Álvarez, and Darío G. Santiago-Pérez, [arXiv:2103.14942](https://arxiv.org/abs/2103.14942).
- [24] This result corresponds to the nonhomogeneous solution of Poisson' equation in the long wave limit and considering the TMD isolated. In order to account for the presence of the environment, we have to include in Eq. (11) the spatial dependence of the dielectric constant on z , $\varepsilon = \varepsilon_T(z)$, i.e., $\varepsilon_T = \varepsilon_1$ if $z < -d/2$, $\varepsilon_T = \varepsilon_2$ for $z > d/2$ and equal to ε_0 in the interval $-d/2 < z < d/2$. The general solution requires us to fulfill the matching boundary conditions at $z = \pm d/2$ [19].
- [25] S. Baroni, S. de Gironcoli, A. Dal Corso, and P. Giannozzi, *Rev. Mod. Phys.* **73**, 515 (2001).
- [26] P. Giannozzi, S. Baroni, N. Bonini, M. Calandra, R. Car, C. Cavazzoni, D. Ceresoli, G. L. Chiarotti, M. Cococcioni, I. Dabo, A. dal Corso, S. de Gironcoli, S. Fabris, G. Fratesi, R. Gebauer, U. Gerstmann, C. Gougousis, A. Kokalj, M. Lazzeri, L. Martin-Samos, N. Marzari *et al.*, *J. Phys.: Condens. Matter* **21**, 395502 (2009).
- [27] J. Klimeš, D. R. Bowler, and A. Michaelides, *Phys. Rev. B* **83**, 195131 (2011).
- [28] J. Klimeš, D. R. Bowler, and A. Michaelides, *J. Phys.: Condens. Matter* **22**, 022201 (2010).
- [29] P. E. Blöchl, *Phys. Rev. B* **50**, 17953 (1994).
- [30] A. Dal Corso, *Comput. Mater. Sci.* **95**, 337 (2014).
- [31] C. Trallero-Giner, A. Cantarero, and M. Cardona, *Phys. Rev. B* **40**, 4030 (1989).
- [32] C. Trallero-Giner, M. Cardona, and F. Iikawa, *Phys. Rev. B* **48**, 5187 (1993).
- [33] Q. Chen, W. Wang, and F. M. Peeters, *J. Appl. Phys.* **123**, 214303 (2018).
- [34] R. Zimmermann and C. Trallero-Giner, *Phys. Rev. B* **56**, 9488 (1997).
- [35] C. Trallero-Giner, F. Iikawa, and M. Cardona, *Phys. Rev. B* **44**, 12815 (1991).
- [36] Th. Sohier, M. Gibertini, M. Calandra, F. Mauri, and N. Marzari, *Nano Lett.* **17**, 3758 (2017).
- [37] Z. Jin, X. Li, J. T. Mullen, and K. W. Kim, *Phys. Rev. B* **90**, 0452422 (2014).
- [38] Z. Huang, W. Zhang, and W. Zhang, *Materials* **9**, 716 (2016).
- [39] A. Chernikov, T. C. Berkelbach, H. M. Hill, A. Rigosi, Y. Li, O. B. Aslan, D. R. Reichman, M. S. Hybertsen, and T. F. Heinz, *Phys. Rev. Lett.* **113**, 076802 (2014).
- [40] K. F. Mak and J. Shan, *Nat. Photonics* **10**, 216 (2016).
- [41] A. Alexandrou, C. Trallero-Giner, G. Kanellis, and M. Cardona, *Phys. Rev. B* **40**, 1013 (1989); A. Alexandrou, C. Trallero-Giner, and A. Cantarero, and M. Cardona, *ibid.* **40**, 1603 (1989).
- [42] D. Li, Ch. Trovatello, S. Dal Conte, M. Nuß, G. Soavi, G. Wang, A. C. Ferrari, G. Cerullo, and T. Brixner, *Nat. Commun.* **11**, 954 (2021).
- [43] N. F. Hinsche and K. S. Thygesen, *2D Materials* **5**, 015009 (2018).
- [44] P. Vogl, *Phys. Rev. B* **13**, 694 (1976).
- [45] M. Cardona, in *Light Scattering in Solids II*, edited by M. Cardona and G. Güntherodt, Topic Appl. Phys. Vol. 50 (Springer, Berlin, Heidelberg, 1982).
- [46] A. Blacha, H. Presting, and M. Cardona, *Phys. Stat. Solidi b* **126**, 11 (1984).
- [47] J. T. Devreese, *Polaron Ionic Crystals and Polar Semiconductors* (North-Holland, Amsterdam, 1972).
- [48] V. L. Gurevich and Yu. A. Firzov, *Zh. Éksp. Teor. Fiz.* **40**, 199 (1961) [*Sov. Phys. JETP* **13**, 137 (1961)]; L. I. Korovin and S. T. Pavlov, **53**, 1708 (1967) [*Sov. Phys. JETP* **26**, 979 (1968)].
- [49] V. López, F. Comas, C. Trallero-Giner, T. Ruf, and M. Cardona, *Phys. Rev. B* **54**, 10502 (1996); F. Iikawa, T. Ruf, and M. Cardona, in *High Magnetic Fields in the Physics of Semiconductors*, edited by D. Heimann (World Scientific, Singapore, 1995).
- [50] D. Christiansen, M. Selig, G. Berghäuser, R. Schmidt, I. Niehues, R. Schneider, A. Arora, S. Michaelis de Vasconcellos, R. Bratschitsch, E. Malic, and A. Knorr, *Phys. Rev. Lett.* **119**, 187402 (2017).
- [51] F. Comas, C. Trallero-Giner, and R. Riera, *Phys. Rev. B* **39**, 5907 (1989).
- [52] G. D. Mahan, *Many-Particle Physics* (Plenum, New York, 1990).
- [53] H. Haken, *Quantum Field Theory of Solids* (North-Holland Publishing, Amsterdam, New York, Oxford, 1976).
- [54] H. Guo, N. Lu, L. Wang, X. Wu, and X. C. Zeng, *J. Phys. Chem. C* **118**, 7242 (2014).
- [55] J.-A. Yan, M. A. Dela Cruz, B. Cook, and K. Varga, *Sci. Rep.* **5**, 16646 (2015).
- [56] L. D. Landau and E. M. Lifschitz, *Course of Theoretical Physics, Vol. 7, Theory of Elasticity* (Oxford, Pergamon, 1970).
- [57] M. Willatzen, L. C. L. Y. Voon, A. N. Gandi, and U. Schwingenschlögl, *Beilstein J. Nanotechnol.* **8**, 1345 (2017).